Estimation of Microscopic Redox Potentials of a Tetraheme Protein, Cytochrome c_3 of *Desulfovibrio vulgaris*, Miyazaki F, and Partial Assignments of Heme Groups†

Kejun Fan,‡ Hideo Akutsu,*,‡ Yoshimasa Kyogoku,§ and Katsumi Niki‡

Department of Physical Chemistry, Faculty of Engineering, Yokohama National University, Hodogaya-ku, Yokohama 240, Japan, and Institute for Protein Research, Osaka University, Suita, Osaka 565, Japan

Received June 6, 1989; Revised Manuscript Received October 24, 1989

ABSTRACT: The microscopic formal redox potentials of a tetraheme protein, cytochrome c_3 from *Desulfovibrio vulgaris*, Miyazaki F, were estimated from the chemical shifts of the heme methyl signals in its ^{1}H NMR spectrum. All chemical shifts in the five macroscopic oxidation states were determined for eight of the heme methyl protons by the saturation-transfer method. The electron-distribution probability at each heme in each oxidation state was estimated directly from the chemical shifts. To minimize errors due to interheme pseudocontact contributions, the average electron-distribution probability was used for calculation of the microscopic formal redox potentials. By introducing interacting potentials, 32 parameters were reduced to 10. The 10 parameters were determined analytically from the 9 independent electron-distribution probabilities and 2 macroscopic formal redox potentials. The results showed the presence of a strong positive interaction between a pair of particular hemes. The microscopic formal redox potential changes dramatically with the extent of reduction because of the intramolecular interheme interactions. NMR signals of two hemes were assigned to particular hemes in the crystal structures by nuclear Overhauser effect experiments. The results showed that the hemes with the highest and lowest redox potentials in the one-electron reduction process correspond to hemes I and IV in the crystal structure.

Cytochrome c_3 isolated from a sulfate-reducing bacterium, *Desulfovibrio vulgaris*, Miyazaki F (*D.v.*MF), is a tetraheme protein that participates in the electron-transfer system involved in the metabolism of sulfur compounds and hydrogen (Postgate, 1984). This protein is of great interest not only from a biological point of view but also because of its physicochemical properties (Yagi et al., 1983). Although the biological functions of four hemes are not yet clarified, the physicochemical properties of this protein were extensively investigated by a variety of methods. The midpoint redox potential was shown to be as low as about −300 mV vs NHE (normal hydrogen electrode) at 25 °C (Niki et al., 1984a), in good agreement with cytochromes c_3 from other sources. The redox mechanism was shown to be a four-consecutive one-electron process, and the four macroscopic formal redox potentials were determined through analysis of its differential pulse polarogram (Niki et al., 1984b) and ^{1}H NMR (Fan et al., 1988, 1989). Mössbauer spectroscopy provided evidence for a strong heme–heme interaction at 4.2 K (Ono et al., 1975). The electrical conduction of a cytochrome c_3 solid thin film containing a trace amount of hydrogenase was found to be very peculiar (Kimura et al., 1979). High conductivity was observed at low temperature and under high hydrogen gas pressure (Nakahara et al., 1980). The difference in ionization potential between the ferric and ferrous forms was as much as 77 kJ/mol, in comparison with 29 kJ/mol for eucaryotic cytochrome *c* (Sato et al., 1980).

Since the electron transfer takes place between two particular hemes, the physicochemical properties of each heme are important to understand the biological functions of the tetraheme protein. One of the most important parameters is the redox potential of each heme, which is called a microscopic redox potential. The thermodynamic redox potential is one of the major factors determining the electron-transfer rate constant (Marcus, 1985). Furthermore, the microscopic redox potentials should reflect the extent of heme–heme interactions. The nature of the microscopic redox potentials and the heme–heme interactions may be elucidated in terms of both physicochemical and structural parameters, since the crystal structure of this molecule has been established by Higuchi and co-workers at 0.18-nm resolution (Higuchi et al., 1984).

A tetraheme protein, such as cytochrome c_3, has five macroscopic oxidation states: the fully oxidized state (S_0) and the one-electron (S_1), two-electron (S_2), three-electron (S_3), and four-electron or fully reduced (S_4) states, as shown in Figure 1. Four macroscopic formal potentials, E^i (i = I, II, III, or IV), can be defined as

$$E = E^i + (RT/F) \ln (f_{i-1}/f_i) \quad (1)$$

where E, R, F, T, and f_i are the equilibrium potential, gas constant, Faraday constant, absolute temperature, and molar fraction of cytochrome c_3 in the i-electron reduced state, respectively. In eq 1, the superscript and subscript i's represent the Roman and Arabic numbers, respectively. When we focus our attention to the redox molecular species, states S_1, S_2, and S_3 contain four, six, and four species, respectively, as shown in Figure 1. Thirty-two microscopic formal potentials (referred to as microscopic redox potentials hereafter) can be defined among these sixteen redox species, as shown in Figure 1 (Sokol et al., 1980; Santos et al., 1984). Here, e_i denotes the microscopic redox potential of heme i. The superscript indicates the reduction step as in macroscopic redox potentials. I and IV show the first and fourth reduction steps, respectively. Since the second and third reduction steps of each heme have multiple pathways, they were described by the combination of the step number (II, III) and the number of hemes that are

† This work was partly supported by the Asahi Glass Foundation for Industrial Technology and the Japan–U.S. Cooperative Science Program of the Japan Society for the Promotion of Science.

‡ Yokohama National University.

§ Osaka University.

0006-2960/90/0429-2257$02.50/0

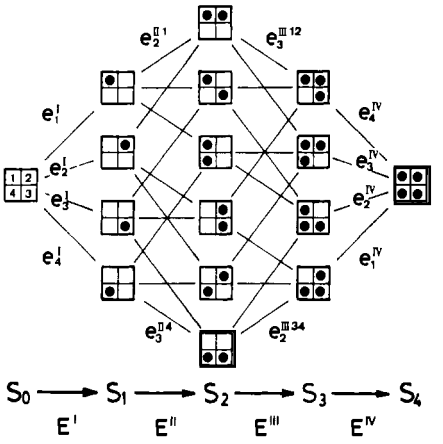

FIGURE 1: Diagram of the five macroscopic oxidation states (S_i) and sixteen redox molecular species (squares). The numbers in the square denote the heme numbers. E^i (i = I–IV) is the macroscopic formal redox potential in the ith reduction step. e_i denotes the microscopic formal redox potential of heme i. The superscript indicates the reduction step as in the case of the macroscopic redox potentials. I and IV show the first and fourth reduction steps, respectively. A combination of step numbers (II, III) and heme numbers (1–4) was used in the superscript to describe the microscopic redox potentials in the second and third reduction steps because of the multiple pathway. For example, III*jk* is the abbreviation of the third reduction step with hemes *j* and *k* kept reduced. According to this principle, the fourth reduction step also can be written as IV*jkl*, which was used only in the case where the reduced hemes should be explicitly specified.

kept reduced during the redox process. For example, III*jk* is the abbreviation of the third reduction step with hemes *j* and *k* kept reduced. According to this principle, the superscript of microscopic redox potential in the fourth reduction step also can be written as IV*jkl*, which was used only in the case where the reduced hemes should be explicitly specified. Microscopic redox potentials were estimated by analyzing the macroscopic redox potentials (Niki et al., 1984a) and by EPR (Gayda et al., 1987) under certain assumptions, where thirty-two microscopic redox potentials were reduced to four. On the other hand, in a pioneering work, Santos et al. (1984) showed that NMR spectroscopy can be used to estimate the relative differences of the microscopic redox potentials and tried to apply it to cytochrome c_3 from *Desulfovibrio gigas*. Since they could not obtain sufficient data and their analysis was not well formulated, their treatments involved methodological and experimental ambiguities. We have carried out more extensive methodological analysis for cytochrome c_3 of *D.v.*MF. We have determined the macroscopic redox potentials through the combined use of NMR and optically transparent thin-layer electrode absorption spectra (Fan et al., 1988, 1989). Using the obtained macroscopic redox potentials and chemical shifts of the heme methyl groups, we could estimate the values of 32 microscopic redox potentials of cytochrome c_3 of *D.v.*MF. Furthermore, we assigned the methyl signals of two hemes to particular heme groups in the crystal structure by nuclear Overhauser experiments, which enabled us to discuss the microscopic redox potentials in the light of the crystal structure.

Experimental Procedures

Desulfovibrio vulgaris, Miyazaki F (*D.v.*MF), was cultured in the medium proposed by Yagi (Yagi et al., 1968). Cytochrome c_3 was purified from cells as reported previously (Yagi & Maruyama, 1971). Its purity was checked with a purity index [A_{552}(reduced)/A_{280}(oxidized) >3.0] and by SDS–polyacrylamide gel electrophoresis. In NMR experiments, a trace amount of *D.v.*MF hydrogenase was added to a 1.2 mM

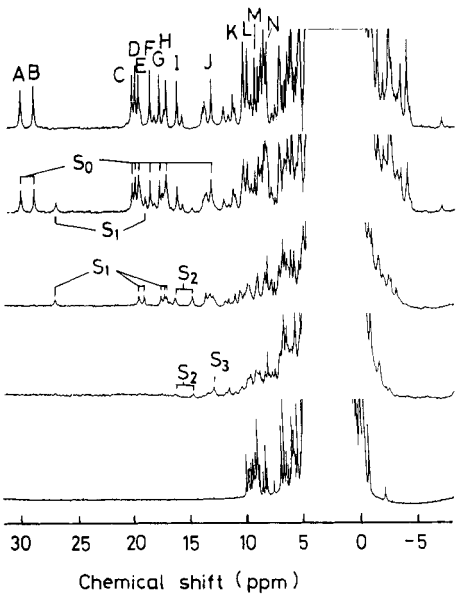

FIGURE 2: 500-MHz ^{1}H NMR spectra of cytochrome c_3 from *D. vulgaris*, Miyazaki F, in a variety of redox stages at 30 °C. The stage of oxidation was changed from the fully oxidized (top) to the fully reduced one (bottom) by changing the hydrogen partial pressure in the presence of hydrogenase. The heme methyl signals are labeled on top. S_i is the macroscopic oxidation state shown in Figure 1.

cytochrome c_3 solution (molar ratio of ca. 0.001) as a redox catalyst. The hydrogenase was kindly supplied by Prof. Yasuoka. Partial reduction (referred to as an intermediate redox stage hereafter) of a cytochrome c_3 solution was achieved by controlling the partial pressure of hydrogen gas in an argon atmosphere in an NMR tube. NMR spectra of cytochrome c_3 were obtained at 30 °C in a 30 mM phosphate buffer solution (p^{2}H 7.1) with JEOL GX-500s and GSX-500 NMR spectrometers. Chemical shifts are presented in parts per million relative to the internal standard 2,2-dimethylsilapentane-5-sulfonate (DSS). Saturation-transfer experiments were carried out for various intermediate redox stages in order to assign heme methyl resonances in the five macroscopic oxidation states. Sixteen free induction decays (FID) were accumulated repeatedly under on-resonance and off-resonance irradiation for 1 s. The irradiation was adjusted to suppress the signal intensity to half the original one. One thousand transients were accumulated for each FID. The nuclear Overhauser effect (NOE) experiments were performed with typically 0.2-s preirradiation and the accumulation of 8000 transients. The difference spectrum was obtained by subtracting the on-resonance FID from the off-resonance FID. Potentials referring to the normal hydrogen electrode are presented in this paper.

Theory

Typical spectra of a cytochrome c_3 (*D.v.*MF) solution in a variety of redox stages are presented in Figure 2. As indicated elsewhere (Fan et al., 1988, 1989), five sets of spectra corresponding to the five macroscopic oxidation states appeared and disappeared one after another. In the intermediate oxidation states, the signals of the heme methyl groups appeared in the region between the positions for the fully oxidized and fully reduced states. Furthermore, only one signal was observed in a saturation-transfer experiment for a specific methyl group in each oxidation state, as shown later. These facts indicate that the transferred electron is delocalized among the four hemes and is hopping around at a rate faster than the NMR time scale (Kimura et al., 1985; Fan et al., 1988, 1989). Thus, the spectra include the information on the electron-

distribution probability at each heme, which can be used for determination of the microscopic redox potentials. Santos et al. (1984) reported an analysis for such a system. We would like to present a brief background and new formulations from our point of view.

When we denote each heme as o (for oxidized) or r (for reduced), the microscopic redox potentials for the first reduction step, e_i^{I} (i = 1–4; heme numbering), can be defined as

$$E = e_1^{\mathrm{I}} + (RT/F) \ln ([\mathrm{oooo}]/[\mathrm{rooo}]) \quad (2)$$

$$E = e_2^{\mathrm{I}} + (RT/F) \ln ([\mathrm{oooo}]/[\mathrm{oroo}]) \quad (3)$$

$$E = e_3^{\mathrm{I}} + (RT/F) \ln ([\mathrm{oooo}]/[\mathrm{ooro}]) \quad (4)$$

$$E = e_4^{\mathrm{I}} + (RT/F) \ln ([\mathrm{oooo}]/[\mathrm{ooor}]) \quad (5)$$

where [oroo], for example, stands for the concentration of the redox species, in which only heme 2 is reduced. From these equations we obtain

$$e_1^{\mathrm{I}} - e_2^{\mathrm{I}} = (RT/F) \ln (R_1^{\mathrm{I}}/R_2^{\mathrm{I}}) \quad (6)$$

$$e_2^{\mathrm{I}} - e_3^{\mathrm{I}} = (RT/F) \ln (R_2^{\mathrm{I}}/R_3^{\mathrm{I}}) \quad (7)$$

$$e_3^{\mathrm{I}} - e_4^{\mathrm{I}} = (RT/F) \ln (R_3^{\mathrm{I}}/R_4^{\mathrm{I}}) \quad (8)$$

where R_i^{I} is the distribution probability of the electron introduced in the first reduction step into heme i. For example, R_1^{I} = [rooo]/([rooo] + [oroo] + [ooro] + [ooor]). Equations 6–8 give the relationships between the microscopic redox potentials to be determined and R_i^j which are observable. Similar equations were obtained for the fourth reduction step, as shown in Appendix I in the supplementary material. Such equations also can be deduced for the second and third reduction steps, respectively. Since $\sum_i R_i^j = 1$ and $\sum_j R_i^j = 1$, only 9 out of 16 R_i^j are independent. If we refer to the macroscopic formal potentials, which were determined previously, additional independent equations can be introduced. From eqs 1–5, we obtain

$$e_i^{\mathrm{I}} = E^{\mathrm{I}} + (RT/F) \ln R_i^{\mathrm{I}} \quad (9)$$

and similarly

$$e_i^{\mathrm{IV}} = E^{\mathrm{IV}} - (RT/F) \ln R_i^{\mathrm{IV}} \quad (10)$$

Consequently, we have 11 independent observations and corresponding equations when we use E^{I} and E^{IV} in addition to R_i^j.

If we assume that the effect of the change in the oxidation state of heme i on the redox potential of heme j, which can be called an interacting potential between hemes i and j, I_{ij}, is not affected by the oxidation states of the other two hemes, any microscopic potential can be described with the four microscopic potentials and six interacting potentials. Thus, 32 parameters can be reduced to 10. Now, we can determine these parameters analytically because we have enough independent equations as shown above.

The interacting potential, I_{ij}, can be defined as (Santos et al., 1984)

$$I_{ij} = e_i^{\mathrm{II}j} - e_i^{\mathrm{I}} = e_i^{\mathrm{III}jk} - e_i^{\mathrm{II}k} = e_i^{\mathrm{IV}}(\text{or } e_i^{\mathrm{V}jkl}) - e_i^{\mathrm{III}kl} \quad (11)$$

where i, j, k, and l denote heme numberings. It follows, for example, that

$$e_i^{\mathrm{IV}} = e_i^{\mathrm{I}} + I_{ij} + I_{ik} + I_{il} \quad (12)$$

and

$$I_{ij} = I_{ji} \quad (13)$$

By use of these relationships, the following equations can be deduced for the second reduction step as shown in Appendix II of the supplementary material

$$l_i Y + m_i(1/Z) + n_i = 0 \ (i = 1\text{–}4) \quad (14)$$

where constants l_i, m_i, and n_i are given in the last part of Appendix II and

$$Y = \exp[(F/RT)(I_{13} - I_{14})] \quad (15)$$

$$Z = \exp[(F/RT)(I_{14} - I_{12})] \quad (16)$$

Equation 14 gives the relationship between the interacting potentials and R_i^j, provided that all of the e_i^{I} are known. In our calculation, we used eqs 9 and 10 to obtain e_i^{I} and e_i^{IV} and then used eqs 12 and 14 to obtain I_{ij}.

The electron-distribution probabilities can be estimated from the chemical shifts of the heme methyl groups for five macroscopic oxidation states. The total paramagnetic shift of heme methyl signal i of heme 1 in the fully oxidized state can be written as (Santos et al., 1984)

$$\delta_1^i = \Delta_{11}^i + \Delta_{12}^i + \Delta_{13}^i + \Delta_{14}^i \quad (17)$$

The intrinsic shift, Δ_{jj}^i, is dominated by the contact contribution. The extrinsic shifts, Δ_{jk}^i ($j \neq k$), can be ascribed to the pseudocontact paramagnetic shifts. For the intermediate oxidation states, the paramagnetic shifts can be given as follows, provided that conformational changes are negligible.

$$\delta_1^i(\mathrm{I}) = \delta_1^i - (R_1^{\mathrm{I}}\Delta_{11}^i + R_2^{\mathrm{I}}\Delta_{12}^i + R_3^{\mathrm{I}}\Delta_{13}^i + R_4^{\mathrm{I}}\Delta_{14}^i) \quad (18)$$

$$\delta_1^i(\mathrm{II}) = \delta_1^i - [(R_1^{\mathrm{I}} + R_1^{\mathrm{II}})\Delta_{11}^i + (R_2^{\mathrm{I}} + R_2^{\mathrm{II}})\Delta_{12}^i + (R_3^{\mathrm{I}} + R_3^{\mathrm{II}})\Delta_{13}^i + (R_4^{\mathrm{I}} + R_4^{\mathrm{II}})\Delta_{14}^i] \quad (19)$$

$$\delta_1^i(\mathrm{III}) = \delta_1^i - [(R_1^{\mathrm{I}} + R_1^{\mathrm{II}} + R_1^{\mathrm{III}})\Delta_{11}^i + (R_2^{\mathrm{I}} + R_2^{\mathrm{II}} + R_2^{\mathrm{III}})\Delta_{12}^i + (R_3^{\mathrm{I}} + R_3^{\mathrm{II}} + R_3^{\mathrm{III}})\Delta_{13}^i + (R_4^{\mathrm{I}} + R_4^{\mathrm{II}} + R_4^{\mathrm{III}})\Delta_{14}^i] \quad (20)$$

Since Δ_{jj} is much larger than Δ_{jk} in general, we may ignore Δ_{jk} ($j \neq k$) in the first step of estimation of the electron-distribution probabilities. This leads to the following simplification.

$$\delta_1^i = \Delta_{11}^i \quad (21)$$

$$\delta_1^i(\mathrm{I}) = \delta_1^i - R_1^{\mathrm{I}}\Delta_{11}^i \quad (22)$$

$$\delta_1^i(\mathrm{II}) = \delta_1^i - (R_1^{\mathrm{I}} + R_1^{\mathrm{II}})\Delta_{11}^i \quad (23)$$

$$\delta_1^i(\mathrm{III}) = \delta_1^i - (R_1^{\mathrm{I}} + R_1^{\mathrm{II}} + R_1^{\mathrm{III}})\Delta_{11}^i \quad (24)$$

Although some of earlier studies suggested a conformational change is induced by the reduction, it would be minor from the geometric point of view, judging from the following arguments. An abnormality in the absorption and CD spectra was observed in the intermediate redox stage in the Soret region (Tabushi et al., 1983; Yagi et al., 1984). However, the abnormality was small and was restricted to the Soret region. The change in the visible absorption spectrum in the other region can be interpreted in terms of a two-oxidation-state model for the entire reduction process. Although a shift of the electron paramagnetic resonance (EPR) signal of one heme was observed on reduction, there was no change for the other hemes (Gayda et al., 1987). It also was established, as mentioned in this section, that the intramolelcular electron exchange is faster than the NMR time scale, suggesting that the conformational change induced by the electron exchange is not significant.

Results

Saturation-transfer experiments were carried out to determine the chemical shifts of the heme methyl groups in the five macroscopic oxidation states. Typically, the irradiation at the heme methyl proton of signal A shown in Figure 3 was carried

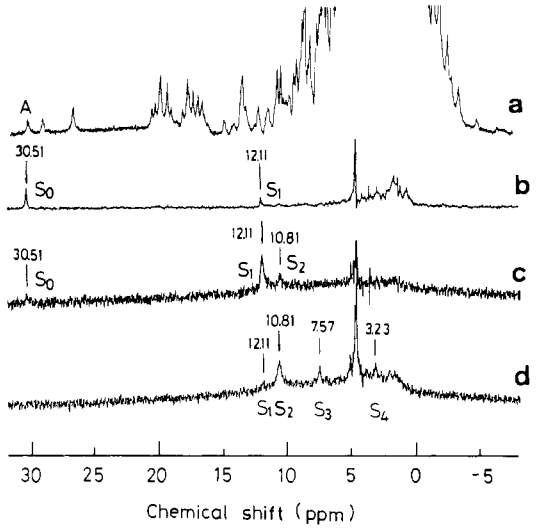

FIGURE 3: Saturation-transfer NMR difference spectra. The signals at 30.51, 12.11, and 10.81 ppm were irradiated with the coexistence of S_0 and S_1 (b), S_0, S_1, and S_2 (c), and S_1, S_2, S_3 and S_4 (d), respectively. (a) is the off-resonance normal spectrum of (b). The chemical shifts are given for signals of interest.

Table I: Chemical Shifts (ppm) of Heme Methyl Signals in the Five Macroscopic Oxidation States at p^{2}H 7.1 and 30 °C

	oxidation state				
signals	S_0	S_1	S_2	S_3	S_4
A	30.51	12.11	10.81	7.57	3.23
B	29.31	26.97	13.06	4.90	3.25
C	20.51	19.83	16.37	6.66	3.15
D	20.24	19.30	14.75	6.03	3.16
E	19.90	16.88	13.46	13.02	3.47
F	18.98	17.70	9.73	4.16	3.26
G	18.07	17.26	8.83	3.78	3.29
H	17.53	7.60	6.77	5.45	3.18
I	16.45	7.35	6.60	5.20	
J	13.52	13.15	11.14		
K	10.62	6.13	5.50		
L	10.35	8.56			
M	9.62	9.25	5.64		
N	8.47	7.07			

out in the coexistence of the molecules belonging to S_0 and S_1. Its normal and saturation-transfer difference spectra are presented in parts a and b, respectively, of Figure 3. The difference spectrum clearly shows that the chemical shift of methyl proton A in the S_1 state is 12.11 ppm. Then the methyl proton at 12.11 ppm was irradiated with the coexistence of the S_0, S_1, and S_2 states. The diffference spectrum in Figure 3c shows that the chemical shift of heme methyl A in the S_2 state is 10.81 ppm. The methyl proton at 10.81 ppm was irradiated with the coexistence of the S_1, S_2, S_3, and S_4 states, as can be seen in Figure 3d. The signals of heme methyl A in S_3 and S_4 appeared at 7.57 and 3.23 ppm, respectively. The obtained chemical shifts for the 14 heme methyl groups are summarized in Table I. The chemical shifts of the eight heme methyl groups (A–H) were identified for all oxidation states.

The electron-distribution probabilities were calculated by using eqs 21–24. Since the observed diamagnetic shifts are quite similar to one another, their average value (3.25 ppm) was used as the diamagnetic shift in the calculation for heme methyl groups I–N. In principle, methyl groups belonging to the same heme should have the same electron-distribution probability. Taking advantage of this property, fourteen heme methyl signals can be classified into four groups. The classified electron-distribution probabilities are given in Table II. The grouping was carried out by using the largest electron-distribution probability in each signal except for heme methyl groups J, N, and L. In the case of the latter, the electron-distribution probability in the first reduction step was used. The electron-distribution probability for the same heme is scattered to a certain extent in Table II, suggesting that the extrinsic paramagnetic shifts are not negligible. Some important conclusions can be deduced from Table II. The electron transferred in each reduction step is actually delocalized among the four hemes. However, we can identify the site keeping the major electron-distribution probability. Namely, hemes 1, 2, 3, and 4 are mainly reduced at the first, second, third, and fourth reduction steps, respectively. Although heme 4 had the second highest electron-distribution probability in the first reduction step, it was mainly reduced in the fourth step. This clearly shows that the existence of the electron at heme 1 affects the redox potential of other hemes significantly and in different way. We can conclude that the interheme interaction plays an important role in the redox potential of each heme, which contradicts the noninteracting models.

Table II: Electron-Distribution Probabilities (R_j^i) Calculated from Heme Methyl Chemical Shifts[a]

heme	signals	R^{I}	R^{II}	R^{III}	R^{IV}
1	A	0.674	0.048	0.119	0.159
	H	0.692	0.058	0.092	0.158
	I	0.689	0.057	0.106	0.145
	K	0.609	0.085		
2	B	0.090	0.534	0.313	0.063
	F	0.081	0.507	0.345	0.057
	G	0.055	0.570	0.342	0.033
	M	0.058	0.567		
3	C	0.039	0.199	0.559	0.202
	D	0.055	0.266	0.511	0.168
	J	0.036	0.191		
4	E	0.184	0.208	0.027	0.581
	L	0.252	0.220		
	N	0.268			

[a] Equations 21–24 were used for calculation. The average value for the observed chemical shifts in the fully reduced state (S_4) was used as the diamagnetic shift for signals I–N. By definition, R_j^i is the distribution probability at heme i of the electron introduced in the jth reduction step. Fourteen heme methyl groups were classified into four hemes according to the largest R^j except for signals J, L, and N. In the latter cases, R^I was used. The four hemes are numbered in the order of the major reduction taking place.

NOE difference spectra with irradiation of the methyl protons of signals A and H–J are presented in Figure 4. On irradiation at the methyl proton at signal A, weak NOE signals were observed at the positions of heme methyl signal H (Figure 4a). The NOE signal at about 9.6 ppm originates from a single proton signal. The irradiation of proton corresponding to signal H also gives an NOE signal at the position of signal A (Figure 4b). As can be seen in Table II, both of the signals A and H belong to heme 1. Since the intraheme NOE can be observed only between the methyl groups at the 1- and 8-positions (Ramaprasad et al., 1984), we can assign signals A and H to either the 1- or 8-methyl group of heme 1. On irradiation of proton at signal I, a strong NOE was observed at signal J and vice versa (Figure 4c,d). Since there is no overlapping at signals I and J, and they belong to hemes 1 and 3, respectively, we can conclude that this is the interheme NOE. The crystal structure of this protein (Higuchi et al., 1984) shows that the shortest interheme methyl carbon distance is 0.417 nm (methyl 5 of heme I–methyl 1 of heme IV; Roman numbers are designations in the crystal structure) and the second shortest one is 0.534 nm (methyl 1 of heme II–methyl 5 of heme III). The former is the only pair that can

Table III: Average Electron-Distribution Probabilities of Four Hemes in the Four Reduction Steps[a]

	R^{I}	R^{II}	R^{III}	R^{IV}	$\sum R^{i}$
heme 1	0.683	0.053	0.105	0.159	1.000
heme 2	0.075	0.537	0.336	0.051	1.000
heme 3	0.047	0.233	0.535	0.185	1.000
heme 4	0.184	0.208	0.027	0.581	1.000
heme 4[b]	0.194	0.170	0.031	0.605	1.000
$\sum$heme i	0.989	1.031	1.003	0.976	
$\sum$heme i[b]	1.000	1.000	1.000	1.000	

[a] Resonances A–H were used in averaging because their chemical shifts were identified for the five oxidation states. [b] Values obtained from $\sum_i R_i^j = 1$.

give rise to a strong NOE signal. Since the NOE experiments mentioned above showed that signal I is neither methyl 1 nor 8, signals I and J can be assigned to the methyl 5 of heme I and methyl 1 of heme IV in the crystal structure, respectively. It leads to the assignment of hemes 1 and 3 to hemes I and IV in the crystal structure, respectively. This assignment is consistent with that inferred on the basis of the crystal structure of heme groups and the results of electrochemistry (Niki et al., 1984a) but contradicts that by EPR (Gayda et al., 1987), which attributed heme 3 to heme II. The assignment of heme 1 is in accord with that for *Desulfovibrio desulfuricans*, Norway, cytochrome c_3 on the basis of chemical modification and electrochemistry (Dolla et al., 1987).

Discussion

Estimation of Microscopic Redox Potentials. The scattered values in Table II showed that the contributions of the extrinsic paramagnetic shifts are not negligible. In the estimation of microscopic redox potentials, the errors in the electron-distribution probability due to the extrinsic paramagnetic shifts should be minimized. For this purpose, the calculated electron-distribution probability was averaged for the methyl groups belonging to the same heme. It was carried out by using the methyl groups, for which all chemicals shifts in the five oxidation states could be identified. They are summarized in Table III. Since the summation for each heme or each reduction step is very close to unity, these values can be used in the calculation of the microscopic redox potentials for the first approximation.

In the first place, e_i^{I} and e_i^{IV} were calculated by using eqs 9 and 10. The results are given in parentheses in Table IV. Then, by a least-squares fitting with eq 14, we obtained

$$I_{13} - I_{14} = 1.1 \pm 0.7 \text{ (mV)} \quad (25)$$

$$I_{14} - I_{12} = -33.4 \pm 0.9 \text{ (mV)} \quad (26)$$

Table IV gives

$$I_{12} + I_{13} + I_{14} = e_1^{IV} - e_1^{I} = -50.9 \text{ (mV)} \quad (27)$$

These three equations gave I_{12}, I_{13}, and I_{14}. I_{23}, I_{24}, and I_{34} could be obtained with eq 12. The interacting potentials also are summarized in parentheses in Table IV.

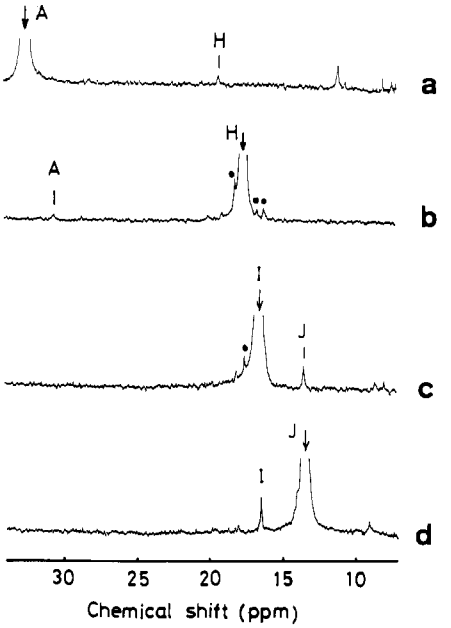

FIGURE 4: NOE difference spectra of cytochrome c_3 in the fully oxidized state at 19 °C (a) and 30 °C (b–d). The arrows indicate the irradiated positions. Definition of the labels is given in Figure 2. A closed circle denotes power spillage. In the case of (a), the measurement was carried out at a lower temperature because a single-proton signal at around 9.6 ppm, which gives an NOE signal, overlapped with heme methyl signal M at 30 °C.

To check the reliability of the estimated redox potentials, the macroscopic redox potentials calculated from them were compared with observed ones. Only E^{II} and E^{III} are independent, since the other two were used in the above calculation. The results are shown in Table IV as well. There were 2- and 3-mV differences for E^{II} and E^{III}, respectively.

As a second approximation step, we modified the electron-distribution probabilities of heme 4 (R_4^j, j = I–IV). Since only one set of R values was obtained for heme 4, there was no averaging process. We modified these values to satisfy that $\sum_i R_i = 1$, as shown by the superscript b's in Table III. The microscopic redox potentials and interacting potentials obtained from the set of modified R values are also summarized in Table IV. These results show better agreement between the observed and calculated macroscopic redox potentials, showing that this is a better set of R values. The 32 microscopic redox potentials calculated from the set of modified R values are shown in a diagram of Figure 5. In view of the reasonable agreement between the calculated and observed macroscopic redox potentials, we may discuss the characteristics of the estimated microscopic redox potentials.

Characteristics of the Microscopic Redox Potentials. A whole set of microscopic redox potentials of cytochrome c_3 was estimated for the first time. It was calculated on the basis of the EPR experiments that the interheme interactions in *D.v.*MF cytochrome c_3 are negligible (Gayda et al., 1987),

Table IV: Microscopic Redox Potentials at the First and Fourth Reduction Steps (e_i^{I} and e_i^{IV}, Respectively) and Interacting Potentials (I_{ij})[a]

microscopic redox potentials (mV)				interacting potentials (mV)		macroscopic potentials (mV)		
							calcd	obsd
e_1^{I}	−270.0 (−270.0)	e_1^{IV}	−320.9 (−320.9)	I_{12}	4.8 (4.9)	E^{I}	−260 (−260)	−260
e_2^{I}	−327.6 (−327.6)	e_2^{IV}	−291.4 (−291.4)	I_{13}	−21.0 (−27.3)	E^{II}	−310 (−309)	−312
e_3^{I}	−339.8 (−339.8)	e_3^{IV}	−324.9 (−324.9)	I_{14}	−34.8 (−28.5)	E^{III}	−327 (−329)	−327
e_4^{I}	−302.8 (−304.3)	e_4^{IV}	−355.9 (−354.8)	I_{23}	42.8 (47.8)	E^{IV}	−369 (−369)	−369
				I_{24}	−11.4 (−16.5)			
				I_{34}	−6.9 (−5.6)			

[a] The values in parentheses were calculated by using the nonmodified electron-distribution probabilities of heme 4. Standard deviation is ±1 mV.

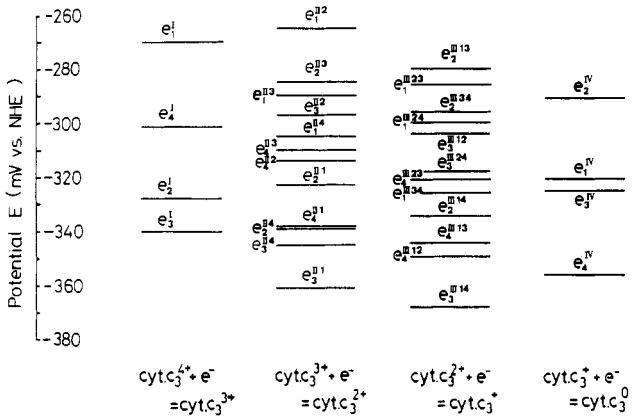

FIGURE 5: Diagram of 32 microscopic redox potentials of cytochrome c_3 estimated by NMR at 30 °C. The nomenclature of the microscopic redox potential of heme i is given in the legend of Figure 1. The reduction process is given at the bottom, where the fully oxidized protein was represented with four positive charges for convenience.

which contradicts our results. It can be said that the analysis of redox potentials on the basis of any noninteracting model is not appropriate. NMR was applied to cytochrome c_3 of *D.v.* Hildenborough at first (Dobson, et al., 1974; Moura et al., 1982). Then, Santos et al. (1984) reported the relative differences of the microscopic redox potentials of cytochrome c_3 from *D. gigas*. However, they used only three signals for the analysis. The small number of observations limited their analysis method, leading to ambiguities (for example, two solutions were obtained for pH 9.6). The relative differences of the macroscopic redox potentials are different from the recent results obtained by polarography (Niviere et al., 1988).

Figure 5 shows that the redox potential of each heme is significantly changed not only in the value but also in the relative order with the change of oxidation state. For example, the redox potential of heme 2 is the second lowest in the first reduction step; it operates as an electron donor. Yet, it becomes the heme with the highest potential in the third and fourth reduction steps and takes on the role of an electron acceptor. In contrast, the redox potential of heme 4 is changed in the opposite direction. This heme has the second highest potential in the first reduction step but becomes the one with the lowest potential in the fourth reduction step. These facts strongly suggest that each heme plays different roles in the different oxidation states. Futhermore, since the microscopic redox potentials are distributed over a wide range (about 100 mV) and the interheme electron exchange within a molecule is rapid, cytochrome c_3 can provide different redox proteins or substrates with multi-electron-transfer paths in a non-equilibrium state. Along with the protein–protein specific recognition, these characteristics could serve as the physicochemical bases for the multifunctionality of this protein in a sulfate-reducing bacterium. Our NOE results showed that the hemes with the highest and lowest potentials in the first reduction step (hemes 1 and 3) are hemes I and IV in the crystal structure, respectively. Heme I has the least exposure to the solvent and is surrounded by the highest positive charge density among four hemes (Higuchi et al., 1984).

The change of the redox potential of each heme was induced by interheme interactions. The remarkable feature of interacting potentials in Table IV is the high positive value of I_{23} ($=I_{32}$). This means that the presence of an electron at heme 2 (or 3) makes the reduction of heme 3 (or 2) much easier. If an electrostatic interaction is the dominant contribution to an interacting potential, only a negative one would be expected. Therefore, a positive interaction should be elucidated in terms of other factors, including structural parameters. A resonance Raman study showed the existence of vibrational exciton coupling among the four hemes of *D.v.*MF cytochrome c_3 (Verma et al., 1988). It was suggested that repulsive forces play a significant role in the interactions in the fully oxidized state, while dispersion forces become more dominant in the fully reduced state. This was discussed in connection with the changes in the inter-iron distances induced by the reduction. Such changes can be reflected in the positive interacting potentials. Our results suggest, however, that the influence of the change is localized to two particular hemes. Such a specifically correlated pair would be expected to originate from a specific conformation of the two hemes in the three-dimensional structure.

It is known that the orientations of the four hemes in the crystal structures are almost identical for cytochrome c_3 from *D. vulgaris*, Miyazaki F, and *D. desulfuricans*, Norway, in spite of their low sequential homology. Two of four hemes (hemes III and IV by the designation in *D.v.*MF crystal structure) are located very close to each other at an almost right angle with an intervening phenylalanine, which is conserved in all cytochromes c_3 so far examined. A specific interaction between these hemes was anticipated by crystallographers (Pierrot et al., 1982; Higuchi et al., 1984). Our NOE results showed that heme 3 in the NMR spectrum is heme IV in the crystal structure, and the interacting potential I_{23} (or I_{32}) has a specific nature. Although the assignment of heme 2 is not yet established, it is highly probable that the positive interheme interaction has something to do with the specific conformation of hemes III and IV in the crystal structure.

Acknowledgments

We are grateful to Prof. N. Yasuoka, Himeji Institute of Technology, for the kind gift of the *D.v.*MF hydrogenase and to JEOL Co. Ltd. for letting us use their facilities.

Supplementary Material Available

Appendix I, giving equations containing the first and fourth reduction steps, and Appendix II, giving the derivation of eq 14 and a full description of the constants (5 pages). Ordering information is given on any current masthead page.

Registry No. Cytochrome c_3, 9035-44-3; heme, 14875-96-8.

References

Dobson, C. M., Hoyle, N. J., Geraldes, C. F., Wright, P. E., Williams, R. J. P., Bruschi, M., & LeGall, J. (1974) *Nature 249*, 425–429.

Dolla, A., Cambillau, C., Bianco, P., Haladjian, J., & Bruschi, M. (1987) *Biochem. Biophys. Res. Commun. 147*, 818–823.

Fan, K., Akutsu, H., Niki, K., Higuchi, N., & Kyogoku, Y. (1988) *J. Chem. Soc. Jpn.*, 512–517.

Fan, K., Akutsu, H., Higuchi, N., Kyogoku, Y., & Niki, K. (1989) *J. Electroanal. Chem.* (in press).

Gayda, J. P., Yagi, T., Benosman, H., & Bertrand, P. (1987) *FEBS Lett. 217*, 57–61.

Higuchi, Y., Kusunoki, M., Matsuura, Y., Yasuoka, N., & Kakudo, M. (1984) *J. Mol. Biol. 172*, 109–139.

Kimura, K., Nakahara, Y., Yagi, T., & Inokuchi, H. (1979) *J. Chem. Phys. 70*, 3317–3323.

Kimura, K., Nakajima, S., Niki, K., & Inokuchi, H. (1985) *Bull. Chem. Soc. Jpn. 58*, 1010–1012.

Marcus, R. A., & Sutin, N. (1985) *Biochim. Biophys. Acta 811*, 265–322.

Moura, J. J. G., Santos, H., Moura, I., LeGall, J., Moore, G. R., Williams, R. J. P., & Xavier, A. V. (1982) *Eur. J. Biochem. 127*, 151–155.

Nakahara, Y., Kimura, K., Inokuchi, H., & Yagi, T. (1980) *Chem. Phys. Lett. 73*, 31–34.
Niki, K., Kawasaki, K., Nishimura, N., Higuchi, Y., Yasuoka, N., & Kakudo, M. (1984a) *J. Electroanal. Chem. 168*, 275–286.
Niki, K., Kobayashi, Y., & Matsuda, H. (1984b) *J. Electroanal. Chem. 178*, 333–341.
Niviere, V., Hatchikian, E. C., Bianco, P., & Haladjian, J. (1988) *Biochim. Biophys. Acta 935*, 34–40.
Ono, K., Kimura, K., Yagi, T., & Inokuchi, H. (1975) *J. Chem. Phys. 63*, 1640–1642.
Pierrot, M., Haser, R., Frey, M., Payan, F., & Astier, J. P. (1982) *J. Biol. Chem. 257*, 14341–14348.
Postgate, J. R. (1984) *The Sulphate-reducing Bacteria*, 2nd ed., p 76, Cambridge University Press, Cambridge, U.K.
Ramaprasad, S., Johnson, R. D., & La Mar, G. N. (1984) *J. Am. Chem. Soc. 106*, 3632–3635.
Santos, H., Moura, J. J. G., LeGall, J., & Xavier, A. V. (1984) *Eur. J. Biochem. 141*, 283–296.
Sato, N., Kimura, K., Inokuchi, H., & Yagi, T. (1980) *Chem. Phys. Lett. 73*, 35–35.
Sokol, F., Evans, D. H., Niki, K., & Yagi, T. (1980) *J. Electroanal. Chem. 108*, 107–115.
Tabushi, I., Nishiya, T., Yagi, T., & Inokuchi, H. (1983) *J. Biochem. 94*, 1375–1385.
Verma, A. L., Kimura, K., Nakamura, A., Yagi, T., & Kitagawa, T. (1988) *J. Am. Chem. Soc. 110*, 6617–6623.
Yagi, T. (1984) *Biochim. Biophys. Acta 767*, 288–294.
Yagi, T., & Maruyama, K. (1971) *Biochim. Biophys. Acta 243*, 214–224.
Yagi, T., Honya, M., & Tamiya, T. (1968) *Biochim. Biophys. Acta 153*, 699–705.
Yagi, T., Inokuchi, H., & Kimura, K. (1983) *Acc. Chem. Res. 16*, 2–7.

Identification of Localized Redox States in Plant-Type Two-Iron Ferredoxins Using the Nuclear Overhauser Effect†

L. B. Dugad and Gerd N. La Mar*
Department of Chemistry, University of California, Davis, California 95616
Lucia Banci and Ivano Bertini
Department of Chemistry, University of Florence, 50121 Florence, Italy
Received August 30, 1989; Revised Manuscript Received October 30, 1989

ABSTRACT: The homonuclear Overhauser effect (NOE), in conjunction with nonselective spin–lattice relaxation measurements, has been employed to assign the contact-shifted resonances for the reduced form of two typical plant-type two-iron ferredoxins from the algae *Spirulina platensis* and *Porphyra umbilicalis*. These results demonstrate that the NOE should have broad general applicability for the assignments and electronic structural elucidation of diverse subclasses of paramagnetic iron–sulfur cluster proteins. NOE connectivities were detected only among sets of resonances exhibiting characteristically different deviations from Curie behavior, providing strong support for the applicability of the spin Hamiltonian formulation for the NMR properties of the antiferromagnetically coupled iron clusters [Dunham, W. R., Palmer, G., Sands, R. H., & Bearden, A. J. (1971) *Biochim. Biophys. Acta 253*, 373–384; Banci, L., Bertini, I., & Luchinat, C. (1989) *Struct. Bonding* (in press)]. The geminal β-methylene protons for the two cysteines bound to the iron(II) center were clearly identified, as well as the $C_\alpha H$ and one $C_\beta H$ for each of the cysteines bound to the iron(III). The identification of the iron bound to cysteines 41 and 46 as the iron(II) in the reduced protein was effected on the basis of dipolar contacts between the bound cysteines, as predicted by crystal coordinates of *S. platensis* Fd [Tsukihara, T., Fukuyama, K., Nakamura, M., Katsube, Y., Tanaka, N., Kakudo, M., Wada, K., Hase, T., & Matsubara, H. (1981) *J. Biochem. (Tokyo) 90*, 1763–1773]. Resolved labile proton contact-shifted resonances are attributed to hydrogen bonding to the iron(III) center, and it is concluded that the contact-shifted resonances for the more numerous hydrogen bonds to the iron(II) center are not resolved from the diamagnetic envelope. The identification of the iron closer to the protein surface as the more reducible one is consistent with predictions based on a larger number of hydrogen bonds to this center.

The iron–sulfur proteins comprise a family of proteins with a remarkable variation in both prosthetic group configuration and redox potential (Orme-Johnson & Orme-Johnson, 1982; Thomson, 1985; Jensen, 1987). Except for the unique one-iron rubredoxins, the prosthetic group usually comprises a cluster of two or four irons and an equal number of labile inorganic sulfurs. Although there are now known systems where the terminal amino acid ligands are not cysteine thiolates (Gurbiel et al., 1989), the classical electron-transfer Fe_2S_2, as well as the Fe_4S_4, cluster proteins possess four coordinated cysteines. A number of less regular three-iron clusters have also been characterized recently (Jensen, 1987). One of the remarkable properties of these iron–sulfur cluster proteins is the wide range of redox potential exhibited even within a family of proteins possessing essentially the same cluster (Carter, 1977). Not

† This research was supported by a grant from the National Science Foundation, DMB-87-03611.

0006-2960/90/0429-2263$02.50/0